AAS 14-267

SOLAR SAIL TRANSFERS FROM EARTH TO THE LUNAR VICINITY IN THE CIRCULAR RESTRICTED PROBLEM

Ashwati Das-Stuart[*], Kathleen Howell[†]

The lunar region enables a variety of mission scenarios that advance space exploration. However, a return to this region of space implies the development of alternative strategies to support affordable mission design options subject to limited resource utilization. Hence, a general solar sail framework is developed to probe the capabilities associated with transfer options employing natural pathways. Prior investigations related to Earth-escape strategies, low thrust regimes and the development of desirable destination orbits at/near a primary all contribute. But, realistic mission constraints such as current sail technology levels, sail inefficiencies, occultation events and limitations on sail maneuverability all impact performance.

INTRODUCTION

The lunar region offers the potential to undertake scientific exploration as well as evaluate human endurance, communications protocols, technology readiness levels, and cargo delivery systems. Such potential ventures have rekindled the interests of the scientific and engineering communities to return to the lunar region in the near future. The desire to sustain a continuous presence near the Moon has re-catalyzed inquiry into novel technologies, such as solar sails, to exploit scarce resources and support extended mission durations. While various strategies have been investigated to escape the Earth in a propellant-less fashion using solar sails, reliable techniques that enable sail capture into favorable lunar orbits remain a topic of research. Thus, a general framework is developed that examines the trade-space for such sail transfers in terms of feasibility, and the associated physical and technical challenges. The transfers are constructed in three phases - a spiral Earth escape, a transit interval and, finally, a capture into a desirable orbit in the vicinity of the Moon.

Spiral escapes using using solar sails has been widely investigated since the 1960's. Sands[1] and Fimple[2] incorporate simplifying assumptions such as a fixed Sun direction, whereas Sackett and Edelbaum[3] as well as Green[4] introduce a rotating Sun line. The fidelity of these models are improved by incorporating J_2[5] and solar gravity[6] perturbations, as well as eclipse events.[5–7] Attempts to improve the performance during the spirals have led to various implementations of a locally optimal steering law to maximize the energy of the orbit and escape the Earth.[5–8] Hartmann[9] identifies such energy-optimal trajectories, developed using small sail accelerations ($< 1\ mm/s^2$), as being comparable to their time-optimal counterparts. Interestingly, when constructing the locally optimal solar sail spiral Earth escapes, many researchers observe a rapid rise in the eccentricity followed promptly by intersections with the surface of the central primary. Therefore, a penalty function is

[*]Ph.D. Student, Purdue University, School of Aeronautics and Astronautics, 701 W. Stadium Ave., West Lafayette, IN, 47906, (412) 294-7541, das15@purdue.edu.

[†]Hsu Lo Distinguished Professor of Aeronautics and Astronautics, Purdue University, School of Aeronautics and Astronautics, 701 W. Stadium Ave., West Lafayette, IN, 47906, (765) 494-5786, howell@purdue.edu.

introduced to increase the radius of pericenter, often at the cost of an increased flight time.[3,7] Other sail steering implementations such as directing the sail acceleration along the velocity vector to escape the Earth have also been investigated.[10–12] In such cases, sail maneuvering close to apoapsis is avoided to prevent excessive lowering of the periapsis.

The second and third phases of a typical sail-enabled Earth-to-Moon transfer path, i.e., the transit interval and capture into a desirable orbit, have also been studied to various degrees. In terms of propulsive capabilities, investigations of impulsive maneuvers, i.e., ΔVs that have enabled time-critical missions to the Moon, have given way to investigations of low thrust systems that support more flexible operational timelines and lowered costs. However, this advantage typically comes at the expense of longer transfer durations. Previous studies into the conventional low thrust transfers to the lunar vicinity offer insights into the design space for the use of solar sails.[10,11,13–15]

The present work aims to combine these separate elements to explore the feasibility of establishing options for efficient, yet timely, transfers between the Earth and the Moon using solar sails. Factors such as sail acceleration levels are varied to assess the impact of currently available and future sail technology. Three steering strategies in this analysis include the Locally Optimal Steering Law (LOSL), the On/Off Steering Law (OFSL) and the Velocity Tangent Steering Law (VTSL). Physical and operational considerations such as a rotating Sun line, eclipsing events, sail inefficiencies, and maintenance of a minimum altitude above the primary are also incorporated into the investigation. The demands on sail turn rates are also explored to identify the technical challenges in the development of realistic solar sail mission scenarios. Baseline trajectory solutions are realized by exploiting solar sail dynamics in combination with advantageous transfer options offered in an Earth-Moon Circular Restricted Three-Body (CR3B) dynamical model. The applicability of the general framework to various transfer scenarios is demonstrated by incorporating a variety of target destinations in the lunar vicinity, including periodic Earth-Moon libration point orbits as well as lunar-centric long-term capture orbits. Depending on the target orbit, natural flow structures (e.g., invariant manifolds) may be available to reduce maneuverability requirements on the sail; alternatively, the sail might be employed to establish the complete end-to-end transfer. The algorithms are formulated as generally as possible to be adaptable to a multitude of transfer scenarios and planetary systems.

SYSTEM DYNAMICAL AND PHYSICAL MODEL

Given a sail moving in the vicinity of both the Earth and the Moon, the gravitational influences of both bodies on the sail are incorporated using the CR3B dynamical model. For the sake of convenience, the equations of motion are developed in the Earth-Moon rotating frame. In this view, the incoming Sun rays are parallel, and inclined approximately 5° to the Earth-Moon invariant plane. These parameters are displayed in Fig. 1. The sail normal, $\hat{n}$, defines the direction of the sail force, a net result from the incident and reflected photons on the sail surface. For a perfectly reflecting surface, the resultant force of the photons acts perpendicular to the sail face. As apparent in Fig. 1, the angles α and δ locate the sail normal in spherical coordinates relative to the Sun line. Note that, it is physically impossible to generate sail forces in a Sunward direction, thus the sail normal must always be directed away from the Sun. The associated non-dimensional equations of motion, as

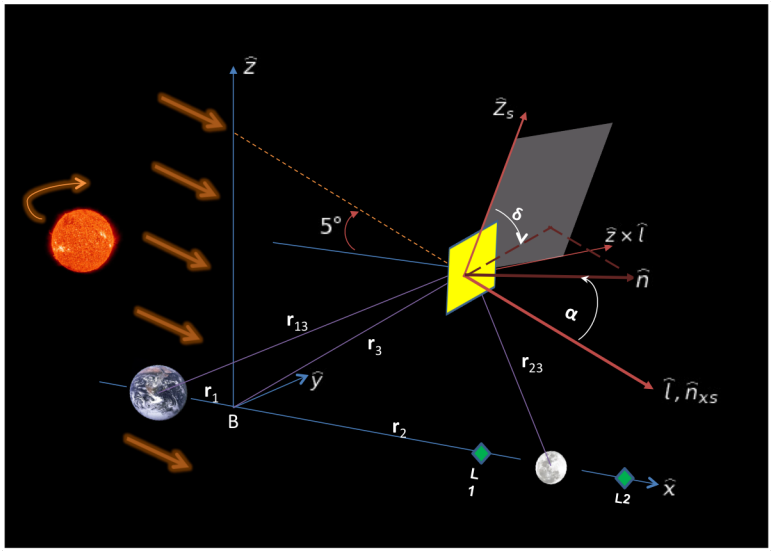

Figure 1. Solar sail in the CR3B Dynamical Model

derived in the Earth-Moon rotating frame, are then written as follows:

$$\ddot{x} = 2\dot{y} + \frac{\partial U^*}{\partial x} + \beta(n_X^3 c_{\Omega t} + n_X^2 n_Y s_{\Omega t}) \tag{1a}$$

$$\ddot{y} = -2\dot{x} + \frac{\partial U^*}{\partial y} + \beta(-n_X^3 s_{\Omega t} + n_X^2 n_Y c_{\Omega t}) \tag{1b}$$

$$\ddot{z} = \frac{\partial U^*}{\partial z} + \beta(n_X^2 n_Z) \tag{1c}$$

where U^* is the pseudo-potential term for the Circular Restricted Three-Body Problem (CR3BP):

$$U^*(x, y, z) = \frac{1-\mu}{r_{13}} + \frac{\mu}{r_{23}} + \frac{1}{2}(x^2 + y^2) \tag{2}$$

and is a function of the relative location of the sail from both the Earth and the Moon, $\boldsymbol{r}_{13}$ and $\boldsymbol{r}_{23}$, respectively. Also, β is the non-dimensional form of the sail characteristic acceleration term, a_c:

$$a_c = \frac{2P\eta}{\sigma} = \frac{9.12\eta}{\sigma[gm^{-2}]}[mm\ s^{-2}] \tag{3}$$

where the mass-to-area ratio is

$$\sigma = \frac{m_t}{A_s} \tag{4}$$

m_t is the total spacecraft mass and A_s is the sail area. The solar radiation pressure, *P*, is assumed to be constant and equal to $4.56 \times 10^{-6}\ N/m^2$ in the Earth-Moon vicinity. The characteristic acceleration, a_c, is the acceleration that a sail with a certain efficiency, η, is capable of providing at 1AU when the sail is fully 'on' (i.e., when the sail normal is oriented along the Sun line; $\alpha = 0°$). JAXA's *IKAROS* sailcraft[16] possessed an a_c value equal to $0.004\ mm/s^2$ and NASA's *NanoSail-D2* sailcraft[17] characteristic acceleration was evaluated to equal $0.02\ mm/s^2$. At the present time, sail technology can only deliver a_c values below $0.1\ mm/s^2$. The total useful sail acceleration is also a

function of the heliocentric distance and the sail orientation from the Sun line, and is expressed as a vector:

$$\boldsymbol{a}_s = a_c \left(\frac{R_E}{r}\right)^2 \cos^2\alpha\, \hat{n} \tag{5}$$

where R_E is the Sun-Earth distance and *r* is the heliocentric distance of the sail, typically approximated as R_E for mission planning at/near the Earth. For convenience, Eqn. (5) is expressed in terms of relevant directions in the Earth-Moon system as:

$$\boldsymbol{a}_s = a_c(\hat{n}^T\, \hat{l})^2 \hat{n} \tag{6}$$

where, $n^T = [n_{X_s}\ n_{Y_s}\ n_{Z_s}]$ and $\hat{l} = [1\ 0\ 0]^T$ are the components of the sail normal and Sun line in the Sun-fixed frame, respectively. Note that $\hat{l}^T\hat{n} = n_{X_s} \geq 0$, as the sail normal is never allowed to assume a Sunward pointing direction. If $\hat{l}^T\hat{n} = 0$, then the sail normal is oriented perpendicular to the Sun line and is, therefore, turned off. Turning the sail off in this manner, such that no sail forces are generated is also termed 'feathering'. In this analysis, multiple transfer scenarios are generated by varying the a_c values to understand the influence of sail efficiencies and physical sail characteristics on performance. The implementation of the different steering laws require varying responses for the total useful sail acceleration, $\boldsymbol{a}_s$ as the steering dictates different deviations (α) of $\hat{n}$ from the Sun line and therefore, different sail orientation histories.

SAIL STEERING LAWS

The sail orientation with respect to the incident photons determines the useful magnitude of acceleration that is harnessed from the sail and also dictates the direction of the acceleration vector as generated from the solar radiation pressure. McInnes[18] describes three primary steering laws to maneuver the sail near planet centered orbits - On/Off, velocity tangent and locally optimal steering laws. These central schemes are further developed for the application to sail transfers between the Earth and the Moon in the CR3B model while incorporating a rotating Sun line.

On/Off Steering Law (OFSL)

For solar sails transferring payload between the Earth and the Moon, the simplest steering law orients the sail normal, $\hat{n}$, either parallel to the Sun line, $\hat{l}$, (fully on) or perpendicular to the Sun line (fully off or 'feathered'). These conditions are mathematically formulated as:

$$\hat{l}\cdot\hat{n} = 1 \ \text{ (Fully ON)} \tag{7}$$

$$\hat{l}\cdot\hat{n} = 0 \ \text{ (Fully OFF)} \tag{8}$$

An advantage of such a steering law is clearly the orientation, that is, $\hat{n}$ directly along the Sun line during anti-Sunward motion allows the sail to generate the maximum possible magnitude of sail acceleration within the limits of the physical sail parameters. Mathematically, a non-zero sail acceleration magnitude, a_s, exists for this steering law only when:

$$0 < \left(\hat{l}\cdot\hat{v}\right) \leq 1 \tag{9}$$

Depending on the scenario, however, a deceleration phase may also be required. In decelerating, the sail normal is directed parallel to and along the direction of the solar rays, but only during Sunward motion. The sail acceleration is then non-zero only when:

$$-1 \leq \left(\hat{l}\cdot\hat{v}\right) < 0 \tag{10}$$

Therefore, the velocity direction and the direction to the Sun at a particular instant in time play a key role in determining the acceleration/deceleration intervals for this steering law. If the conditions for the required Sun-velocity direction during the acceleration or deceleration phases are not met, the sail is turned edge-on to the Sun line and is, therefore, fully 'off'.

Velocity-Tangent Steering Law (VTSL)

The maximum magnitude of the acceleration from the On/Off steering law is usually accomplished for a sail oriented toward a direction vastly different from the direction of motion, an orientation that may be undesirable in many circumstances. Rather, the velocity impulse is desired along the velocity direction. Such a sail orientation is achieved by specifying that the sail normal be parallel to the inertial velocity direction, as investigated by Ozimek and Grebow:[10,11]

$$\hat{n} \cdot \hat{v} = 1 \tag{11}$$

The ability to orient the sail normal along the velocity direction does, however, deliver a diminished sail acceleration magnitude due to the deviation of $\hat{n}$ from the Sun line. Consistent with Eqns. (9) and (10), the sail can still accelerate, decelerate or maintain its nominal motion.

Locally Optimal Steering Law (LOSL)

The Locally Optimal Steering Law (LOSL) offers a solution that orients $\hat{n}$ such that the sail acceleration is maximized along the direction of motion.[18] Therefore, the LOSL offers a compromise between the high acceleration magnitude via the OFSL, and the diminished acceleration magnitude but pointing direction advantages available from the VTSL. Differing implementations of the LOSL strategy have been investigated in varying gravitational models and systems by various authors including McInnes,[18] MacDonald and McInnes,[7] Coverstone[6] and Edelbaum.[3] The equations are incorporated and adapted from Coverstone[6] for this investigation in the CR3B model. For the formulation here, at a given instant of time, the energy-maximizing direction is first determined. The sail normal components are derived relative to the Sun line, expressed in the Sun-fixed frame, followed by a transformation into the rotating frame for incorporation into the EOMs. Recall Eqn. (5) for computing the useful sail acceleration in the Earth-Moon system. Assume that $\boldsymbol{\nu}$ represents the velocity vector in the Sun-fixed frame. To maximize the energy in the direction of velocity, $\boldsymbol{\nu}$, the component of sail acceleration is maximized in its direction. Therefore, the goal is the maximization of the quantity, $\boldsymbol{a_s}^T \boldsymbol{\nu}$:

$$\boldsymbol{a_s}^T \boldsymbol{\nu} = a_c(\hat{l} \cdot \hat{n}^T)^2 \hat{n}^T \boldsymbol{\nu} \tag{12}$$

The Hamiltonian for this constrained parameter optimization problem is then posed as:

$$H = a_c(\hat{l}^T\, \hat{n})^2 \hat{n}^T \boldsymbol{\nu} + \lambda(\boldsymbol{n}^T \boldsymbol{n} - 1) \tag{13}$$

where λ is a Lagrange multiplier that adjoins a constraint on the sail normal magnitude with the objective function. With the exception of the Sun pointing constraint, the sail angles are free variables subject to the constraint that the sail normal is of unit magnitude:

$$n_X^2 + n_Y^2 + n_Z^2 = 1 \tag{14}$$

Note that the components in the Sun frame are denoted by the subscripts $[X-Y-Z]$. The maximum of the Hamiltonian with respect to the sail angles results in the sail orientation that maximizes the

energy in the direction of motion. This extremum of the Hamiltonian is evaluated from the first-order necessary condition:

$$\frac{\partial H}{\partial \boldsymbol{n}} = 2a_c(\hat{l}^T\boldsymbol{n})(\boldsymbol{\nu}^T\boldsymbol{n})\hat{l} + a_c(\hat{l}^T\,\boldsymbol{n})^2\boldsymbol{\nu} + 2\lambda\boldsymbol{n} = \mathbf{0} \tag{15}$$

Expanding Eqn. (15) leads to the following relationships with respect to each axis in the Sun-frame coordinate system, that is:

$$2a_c n_X(n_X\nu_X + n_Y\nu_Y + n_Z\nu_Z) + a_c n_X^2\nu_X + 2\lambda n_X = 0 \tag{16}$$

$$a_c n_X^2\nu_Y + 2\lambda n_Y = 0 \tag{17}$$

$$a_c n_X^2\nu_Z + 2\lambda n_Z = 0 \tag{18}$$

Solving for λ in Eqns. (17) and (18) yields:

$$\lambda = \frac{-a_c n_X^2\nu_Y}{2n_Y} = \frac{-a_c n_X^2\nu_Z}{2n_Z} \tag{19}$$

that, once equated, leads to:

$$\frac{n_Z}{n_Y} = \frac{\nu_Z}{\nu_Y} \tag{20}$$

Equation (16) is trivially *zero* when the sail is off, i.e., $n_X = 0$. However, by substituting Eqns. (19) and (20) into Eqn. (16), defining $\zeta = \frac{n_Y}{n_X}$, and solving for ζ, the following quadratic is obtained:

$$\zeta = \frac{-3\nu_X\nu_Y \pm \nu_Y\sqrt{9\nu_X^2 + 8(\nu_Y^2 + \nu_Z^2)}}{4(\nu_Y^2 + \nu_Z^2)}. \tag{21}$$

In Eqn. (21), a '$+$' or '$-$' sign is selected depending upon the value that maximizes the component of the sail acceleration in the velocity direction:

$$\boldsymbol{a_s}^T\boldsymbol{\nu} = a_c n_X^2(n_X\nu_X + n_Y\nu_Y + n_Z\nu_Z) \tag{22}$$

Dividing Eqn. (22) by $a_c n_X^3$, rewriting the equation in terms of ζ, utilizing the relationships in Eqn. (20), and finally substituting ζ from Eqn. (21), leads to the following relationship:

$$\frac{\boldsymbol{a_s}^T\boldsymbol{\nu}}{a_c n_X^3} = \frac{\nu_X}{4} \pm \frac{\sqrt{9\nu_Y^2 + 8(\nu_Y^2 + \nu_Z^2)}}{4} \tag{23}$$

Now, by selecting the '$+$' sign in Eqn. (23), the left side of the equation and, therefore, the sail acceleration in the velocity direction is maximized. To determine the required sail pointing directions, Eqns. (14) and (20) as well as $\frac{n_Y}{n_X} = \zeta$ are used to specify the sail pointing terms in the Sun-fixed frame:

$$n_X = \frac{\|\nu_Y\|}{\sqrt{\nu_Y^2 + \zeta^2(\nu_Y^2 + \nu_Z^2)}} \tag{24}$$

$$n_Y = \zeta n_X \tag{25}$$

$$n_Z = \frac{\nu_Z}{\nu_Y} n_Y \tag{26}$$

Note that all three pointing direction components are coupled and functions of the velocity components relative to the Sun frame. Alternatively, the orbit energy is minimized by using the '$-$' sign in Eqn. (23) and, therefore, in the determination of ζ via Eqn. (21).

TRAJECTORY GENERATION FRAMEWORK

A primary objective in this investigation is the development of a framework to support the construction and analysis of varied types of solar sail transfers for capture into a selection of destination orbits. Transfers to Lyapunov and halo orbits demonstrate the capability to explore planar or spatial scenarios. These examples within the context of the CR3B model, allow an investigation into the advantages and challenges associated with blending the low thrust sail propagation with low energy options that are possible via the manifolds corresponding to the appropriate libration point orbits. The target periodic orbits and their associated manifolds are generated using linear systems theory, in particular, the monodromy matrix and the associated eigenspace. Lunar-centric long term capture orbits are also considered for their potential to support proximity operations or scientific investigations near the Moon. However, the enhanced stability of capture orbits close to the Moon can prohibit the existence of natural flows to/from these orbits. Accordingly, transfers to such orbits offer insight into the capability of the sail to perform end-to-end transfers in the absence of any low energy arcs. The lunar capture orbits are formulated using Poincaré mapping techniques which aid in selecting initial conditions that establish long term capture behavior.

The construction of the Earth-Moon transfers is developed using reverse time propagations, beginning with the transfer leg from the destination orbit, followed by the Earth spiral phase. The reverse time propagations and the order of construction of the phases are motivated by the challenge in matching the end of the sail spiral escape with the beginning of the desired stable manifold or sail-propagated transfer leg to the lunar capture orbit. The time-invariant nature of the stable manifolds in the CR3B model allows greater flexibility in the epoch at which the reverse time Earth escape phase is initiated, thereby offering more options for mission design. In contrast, transfers to the long-term capture orbits are more constrained because the sail-generated capture leg is dependent on the Sun line direction, and, therefore, has time dependent properties. Consequently, the Earth spiral phase is constrained to initiate at the exact time that is associated with the terminal point of the reverse time propagated capture leg. These capture legs from the destination orbits are terminated in the vicinity of the Earth. The Earth escape spirals are initiated from the end of the capture legs and propagated towards the Earth by allowing the sail to initially be active everywhere on the spirals. The propagation is terminated, however, if the sail crosses a minimum altitude boundary of 3000 *km*, which is a design value selected to minimize the influence of the atmosphere during the Earth escape attempts. Following a terminated spiral, the propagation is re-initiated from the capture leg, but this time, the sail is constrained to remain inactive within a certain threshold surrounding the apogee along each spiral leg. The threshold is widened with each iteration of the propagation until the sail achieves an energy level equivalent to that of a two-body Geostationary Transfer Orbit (GTO) with respect to the Earth. Note that the final orbit is not constrained to possess a perigee at LEO, as a traditional GTO. In all the transfer simulations, the implementation differences and the influence of all three steering laws on the transfer performance are explored. Even though the transfers are developed in reverse time, the sail is maneuvered in such a manner that, regardless of the steering law, the sail accelerates when spiraling to escape the Earth and decelerates during capture into the desired lunar orbit in forward time. Therefore, in the case of the VTSL and OFSL, the sail is active only when moving anti-Sunward during the escape phase, and only when traveling Sunward during the capture phase. In contrast, the LOSL orients the sail normal in a direction that maximizes the energy in the velocity direction during the escape phase, and the sail orientation minimizes the energy during the capture phase.

RESULTS - Transfer Trajectories

A subset of Lyapunov and southern halo orbits are selected as targets for this analysis where they range in Jacobi constant values from 3.05 to 3.17. Some physical characteristics such as their size and inclination aid in gaining a physical sense of their presence in the design space. For example, the y-amplitude of the representative Lyapunov orbits covers values from $A_y = 2.15 \times 10^4$ *km* to $A_y = 8.08 \times 10^4$ *km*, whereas the out-of-plane z-amplitudes of the selected southern halo orbits vary between $A_z = 8.61 \times 10^3$ *km* to $A_z = 5.01 \times 10^4$ *km*. Although the Lyapunov orbits are in the plane of the Earth and the Moon, the inclinations of the halo orbits relative to the Earth-Moon plane fall between $\approx 1.5^\circ - 8.8^\circ$. The stable manifolds associated with each of the Lyapunov orbits are constructed from the leftmost intersection of these orbits with the rotating $\hat{x}$ axis. In contrast, the stable manifolds associated with the halo orbits are constructed from their maximum z-amplitude co-ordinates. These stable manifolds are propagated towards the Earth in reverse time and are terminated at the first periapsis crossing in the Earth's vicinity. The manifolds inherit the Jacobi constant values associated with their orbit, so, those emanating from the larger orbits possess lower Jacobi values. The terminal periapses along these manifolds offer the opportunity to test the transfer characteristics in response to a variety of conditions; these may include different energy levels, altitudes, relative position from the Earth, orientations with respect to the Sun line and orbital element characteristics.

The lunar capture orbits are generated at a Jacobi constant value equal to 3.178, simply as an example. The sample orbit illustrated in Fig. 2 passes as close as ≈ 8700 *km* and as far as ≈ 23000 *km* from the Moon's surface, leading to eccentricities between 0.3 and 0.4. The sail forces generated to establish the transfer leg engender varying energy levels throughout the propagation. So, although the lunar centric orbits do not possess asymptotically stable manifolds, the solar sail propagations from these orbits, with terminal points near the Earth, serve the same transfer function.

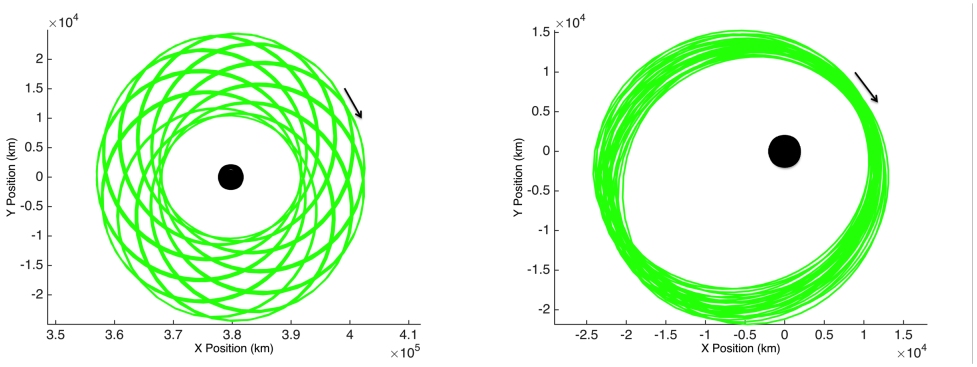

(a) Rotating View (b) Moon Centered-Inertial View

Figure 2. A sample lunar capture orbit propagated for $\approx$ 75 *days*, and visualized in both the Earth-Moon rotating frame (a), and the Moon-centered inertial frame (b).

Specific sample paths are selected to illustrate the geometry and performance associated with the libration point and lunar orbit transfers. Figures 3, 4 and 5 illustrate these characteristics. The specific Lyapunov destination orbit corresponds to a Jacobi constant value approximately equal to ≈ 3.1630 and a period near ≈ 12 *days*. The Lyapunov orbit transfers are computed using a sail with an a_c value of $0.5\ mm/s^2$ whereas the longer transfer to the Moon is tested using a smaller a_c value, i.e., $0.3\ mm/s^2$. Both sails are assumed to be a 100% efficient. The illustrated results

are not intended as a direct comparison of the libration point and lunar orbit transfers. Instead, they are intended to highlight the nuances associated with both types of transfer. Figures 3(a)-3(b) display the ability of the solar sail framework to accommodate transfer architectures regardless of the combination of low thrust and low energy mechanisms. In Fig. 3(b), note the blending of

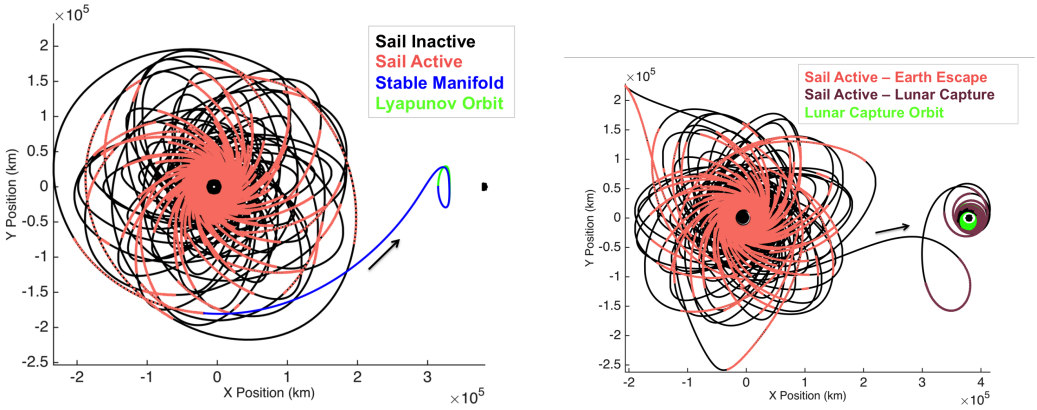

(a) OFSL (b) OFSL escape+VTSL capture

Figure 3. Rotating frame view profiles associated with spiral Earth escapes and insertion into an L_1 Lyapunov (a), and a long-term lunar capture orbit (b). The arrow indicates the direction of motion in forward time.

different steering laws to execute an end to end transfer - the OFSL enables the Earth escape while the VTSL accomplishes the Moon capture. Although the OFSL is employed for Earth escape in both Figs. 3(a) and 3(b), the varied conditions on both the manifold (a) and sail propagated (b) terminal points effects a different geometry for each spiral scenario. Although the rotating frame conditions enable the generation of such baseline solutions, it is challenging to gain an intuitive understanding of the behavior and characteristics of the transfer in this view. The inertial frame views (Fig. 4) however illustrate a more familiar and intuitive visual representation of the transfers.

The Earth escape in Fig. 4(a) is enabled by the LOSL, followed by a natural capture into the Lyapunov orbit. In Fig. 4(b), the sail-propagated Earth escape and Moon capture phases are both implemented using the VTSL. This comparison exhibits the superiority of the LOSL under the specified conditions, in allowing greater opportunities for an active sail during the spiral phase; the steering law does not enforce sail feathering (turning off the sail) during Sunward motion, unlike the VTSL and OFSL. These inertial views also offer perspectives on the varying orbital elements such as eccentricity and semi-major axis. The different orientations of the line of apsides also observed, as the orientation of the periapses shift with the progression of the spirals in reverse time.

The altitude profile along the orbits as they move through the spiral Earth escape and orbit capture phases are plotted in Figs. 5. The negative time in Figs. 5(a) and 5(b) indicate reverse time propagations. Recall that the reverse time propagations are motivated by the challenge in matching the end of the escape spiral with the beginning of the transfer arcs to the destination orbits. Thus, in Figs. 5(a), the negative time conveys the time to arrival at the terminal point along the stable manifold at time 'zero'. The sail then travels on the stable manifold for ≈ 18 *days* till it naturally captures into the destination Lyapunov orbit. Unlike the time invariant stable manifold, the time varying nature of the path during the sail-propagated Moon capture phase is unable to be shifted to render a terminal point at time 'zero'. Therefore, in Fig. 5(b), the negative time encompasses the time

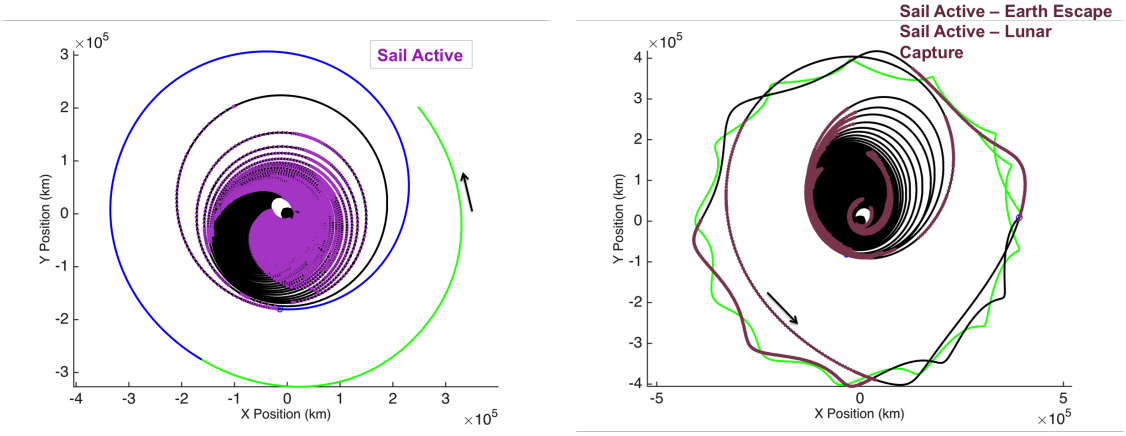

(a) LOSL (b) VTSL escape+VTSL capture

Figure 4. Inertial frame view profiles associated with spiral Earth escapes and insertion into an L_1 Lyapunov (a), and a long-term lunar capture orbit (b). The arrow indicates the direction of motion in forward time.

to escape Earth, followed by capture into the lunar orbit at time 'zero'. As mentioned earlier, approaching the Earth in negative time and allowing sail forces to be generated near apogee creates the potential to induce orbits with high eccentricity. So, the sail is switched off within specified bounds surrounding the apogee of each spiral to prevent rapid lowering of the perigee and, therefore, avoid a premature crash into the primary. Considering the reverse time propagations, the altitude along the path is reduced using sail forces from orbits with apogee altitudes near $350,000$ *km* and perigee altitudes close to $150,000$ *km*, to those with perigee altitudes above 3000 *km* and apogee altitudes on the order of $30,000$ *km*. The final condition in reverse time leads to a two-body GTO energy with respect to the Earth (approximately -8.307 $\frac{km^2}{s^2}$). Each cycle in the altitude profile is indicative of certain orbital characteristics such as the size. Consistent with Figs. 4, the spirals evolve into orbits that are smaller as they approach the Earth in reverse time. Observe the times-of-flight (TOFs) from the Earth to the destination orbits in Fig. 5. They illustrate that the transfer displayed in Fig. 4(a)

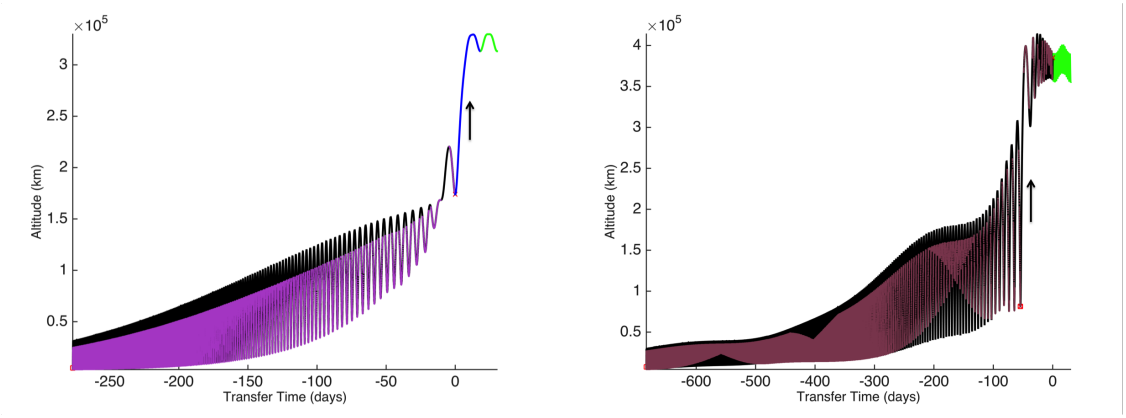

(a) LOSL (b) VTSL escape+VTSL capture

Figure 5. Altitude profiles associated with spiral Earth escapes and insertion into an L_1 Lyapunov (a), and a long-term lunar capture orbit (b). The arrow indicates the direction of motion in forward time.

is accomplished in ≈ 300 days whereas, Fig. 4(b) illustrates a path that requires ≈ 700 days, with the Earth escape phase as the major contributor at 650 days. The difference of ≈ 350 days in the Earth escape phase between the libration point orbit and the Moon capture orbit transfers arises due to various factors such as: the varied energy, the orbit conditions, and the Sun line direction at the initiation of the spirals; the varied maximum-acceleration-generating capabilities of the sails; and the different steering laws. For example, the duration of the Earth escape phase in Fig. 5(b) can be shortened by ≈ 250 days by employing the LOSL instead of the VTSL. Such a performance boost is possible when allowing the sail more opportunities to be active during the spirals, in addition to the higher acceleration magnitudes using the LOSL.

To gain a more general understanding of the trade space comprised of sail a_c values and the steering law influences, Figs. 6 illustrate the TOFs as a function of these variable types of inputs. The a_c values that are selected incorporate a current capability in sail technology of $0.1\ mm/s^2$ to values that are more consistent with future developments such as $0.5\ mm/s^2$. The Jacobi constant (JC) in these figures identifies a unique member of the specific subset of Lyapunov and halo families. Perhaps not surprisingly, both figures display a decreasing trend in TOF with increasing

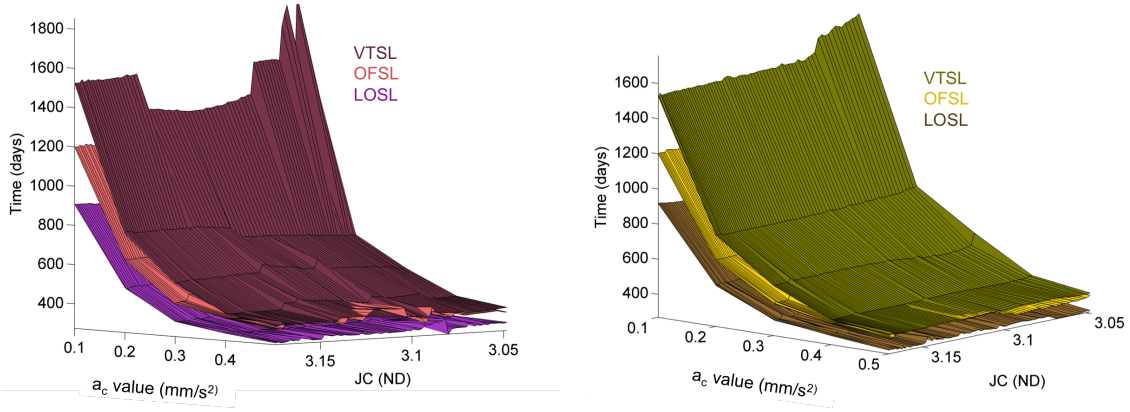

(a) Lyapunov transfers

(b) Halo transfers

Figure 6. Surface plots for transfer times associated with transfers to a subset of Lyapunov (a), and halo orbits (b), over a range of sail a_c values and varying steering laws.

sail acceleration magnitudes. Given an upper bound on current sail technology at $\approx 0.1\ mm/s^2$, the transfers are accomplished in about 4 years using the VTSL. Interestingly, only about half this duration is typically required when employing the LOSL. As discussed earlier, the VTSL transfers possess the longest TOFs due to two contributing factors: (i) an inability to generate sail forces during Sunward motion, and (ii) a diminished acceleration magnitude engendered by the deviation of the sail normal from the Sun line. For a given steering law and a_c value, the transfer durations to the orbits within the Lyapunov family seem comparable. The same is true for transfers to members of the halo family. Long flight durations appear to be offset by the ability to complete the transfers with no propellant, and, therefore, lower associated launch mass. Overlaying the Lyapunov and halo orbit TOF surfaces displayed in Figs. 6(a) and 6(b) indicate that the TOFs corresponding to both the Lyapunov and halo transfers seem comparable across the selected range of Jacobi constant values. However, greater inclinations and eccentricities associated with transfers to the larger halo orbits and their manifolds, as well as their proximity to the Earth, render these transfers vulnera-

ble to a rapid perigee drop in reverse time. To compensate for such an undesirable outcome, the apogee cut-off, bounding the time to feather the sail, are wider for these halo transfers as compared to Lyapunov transfers at similar energy levels. Consequently, expanded opportunities to maintain an active sail also renders the Lyapunov transfers shorter than transfers to the halo orbits at those similar energy levels. Such observations offer insight into the impact on vehicle performance.

The regions that describe the apogee cut-off bounds are also expressed in terms of sail active fractions in a given orbit. These fractions are defined as a specified percentage of the most recent apogee passage altitude. The current spiral characteristics do not vary significantly from its predecessor, true for the majority of the spiral phase constructed using the low-thrust. Figures 7 display the sail active fractions for each steering law that enables the solutions in Figs. 6. As an example,

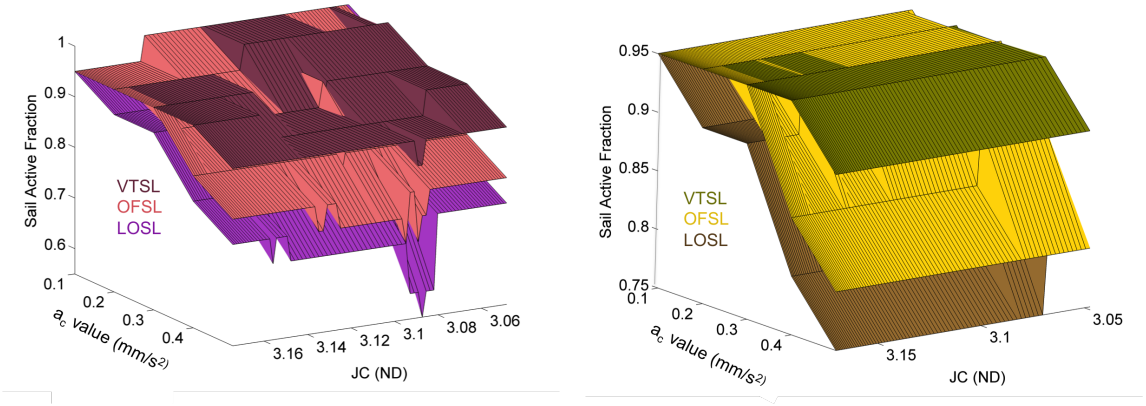

(a) Lyapunov transfers (b) Halo transfers

Figure 7. Surface plots for allowable sail active fractions associated with transfers to a subset of Lyapunov (a), and halo orbits (b), over a range of sail a_c values and varying steering laws.

a sail active fraction of 0.9 implies that the sail is active below a 10% bound on the apogee altitude associated with the previous spiral, providing such active status does not violate the steering law. Lower sail active fractions are required to produce a more gentle lowering of the periapses on the Earth escape spirals, in reverse time, with a high eccentricity due to the transfer leg terminal conditions, the steering law and the acceleration capability of the sail (a_c value). As can be observed, the fraction is generally smaller for higher a_c values - greater acceleration magnitudes tend to more swiftly reduce the perigee altitude in reverse time. The diminished acceleration magnitude associated with the VTSL steering law naturally favors a more gradual reduction in the perigee altitude and thus, in general, allows for higher sail active fractions.

Influence of Shadows

Shadow regions pose an additional challenge for solar sail transfers because the sail's ability to generate acceleration is inhibited depending on the amount of available sunlight. The Sun-Earth-Moon geometry gives rise to three shadow regions each for the Earth and Moon, namely the partially lit penumbra and antumbra regions, and the completely photon-starved umbra region. Only the effects of the Earth-Moon umbra cones, where the sail is incapable of generating any sail forces, are incorporated in this preliminary investigation. A schematic of the relevant umbra regions, direction vectors and angles appear in Fig. 8. The subscripts E, M, SS and U in the figure correspond to

Earth, *Moon*, *Solar Sail* and the *Umbra* region, respectively. Since the Sun is modeled as a point source, its rays intercept the sail at approximately 0.15° with respect to the Earth-Moon barycenter line, when the sail is at an Earth-Moon distance perpendicular to this line. As a worst case scenario, the Sun intercepts the sail at approximately 0.30° at two Earth-Moon radii under the same geometry conditions. Since these angles are small, the incoming rays are modeled as parallel, certainly a reasonable assumption in the CR3B model. However, the umbra regions are modeled as cones rather than cylinders to offer a slightly more representative analysis of the possible shadow encounters in the vicinity of the Earth and the Moon. The mid-line of the two modeled umbra cones remain parallel, consistent with the incoming Sun's rays. The terminal points of the shadow cones, U_E

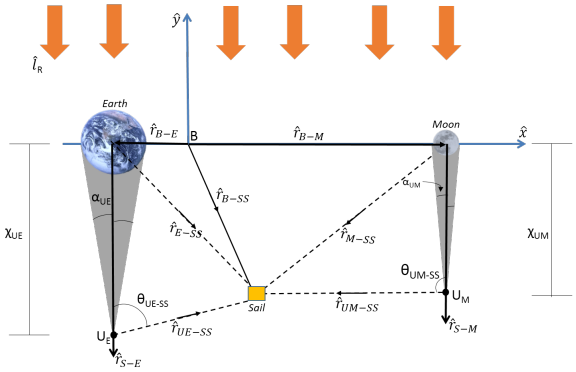

Figure 8. Earth-Moon umbra shadow regions in the rotating frame

and U_M are located at distances of $X_{UE} = 1.385 \times 10^6$ *km* and $X_{UM} = 3.748 \times 10^5$ *km* from their respective primaries. The sail is identified as being in shadow when (i) $\theta_{UE-SS} \leq \alpha_{UE}$ or $\theta_{UM-SS} \leq \alpha_{UM}$; and (ii) when the sail is opposite to the Sun location relative to the primaries, i.e., when $\cos^{-1}(\hat{l}_R \cdot \hat{r}_{E-SS}) \leq 90^\circ$ or $\cos^{-1}(\hat{l}_R \cdot \hat{r}_{M-SS}) \leq 90^\circ$. When in shadow, the sail motion is solely governed by the natural, classical CR3B model EOMs, and is equivalent to the sail normal being feathered with the cone angle $\alpha = 90^\circ$. The influence of these shadow events on the sail performance is highlighted in Fig. 9. A visual comparison of Figs. 4(a) and 9(a) demonstrates

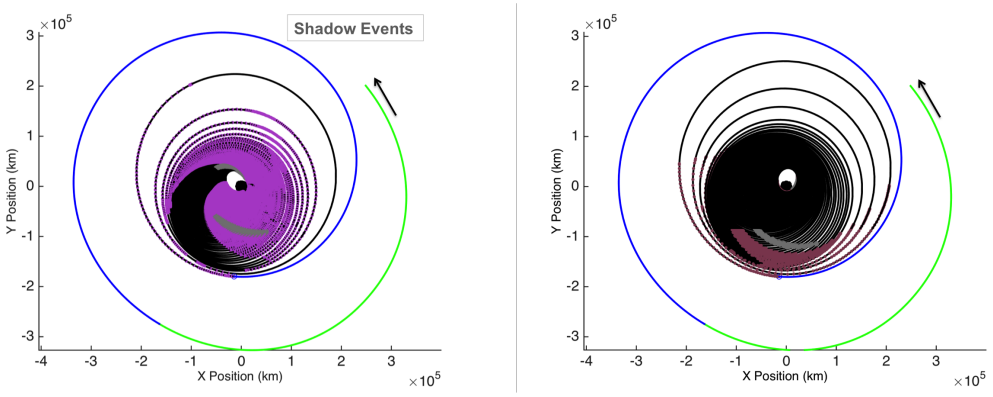

(a) Locally optimal (b) Velocity tangent

Figure 9. Inertial frame view profiles associated with a spiral Earth escape and insertion into an L_1 Lyapunov orbit with Jacobi constant ≈ 3.1630, in the presence of shadow events. The arrow indicates the direction of motion in forward time.

Table 1. TOF increases from incorporating occultation - Earth to Lunar orbit capture

Earth Escape Spiral ($a_c = 0.3\ mm/s^2$)			
Steering Strategy	TOF - No Shadow (days)	ΔTOF - With Shadow (days)	$\%$ Increase
VTSL	630	+6	+1
OFSL	552	+13	+2
LOSL	387	+37	+10
Moon Capture Phase ($a_c = 0.3\ mm/s^2$)			
VTSL	54	+0	+0

that the basic geometry of the transfers does not necessarily change upon introducing occultation events. Although each scenario is different, these sample cases explore the ability of occultation events to prolong the transfer duration. An assessment of the TOFs for the transfers to the specific Lyapunov orbit in Figs. 9, incorporating occultation events demonstrates that the transfer duration is increased by $\approx$ 8 days for the LOSL enabled transfer, an increase of $\approx$ 20 days occurs for the OFSL (not shown) and the TOF increase is $\approx$ 11 days for the VTSL. These results correspond to approximately $+3\%$ increases in TOFs for both the LOSL and VTSL and approximately a $+5\%$ increase for the OFSL. The implication of the results depends on the interpretation, so caution is warranted. It initially appears that the higher level sail-active-opportunities with the LOSL, implies that it is more vulnerable to shadow events. In contrast, the fact that the sail is inactive along multiple segments along the spiral could render the VTSL and OFSL trajectories less vulnerable to the effects of shadow than the LOSL transfers. However, in the example, the OFSL trajectory suffers the greatest increase in flight duration due to shadow, whereas the increases in TOF for the VTSL and LOSL are more comparable. The results from the next example further support the fact that the effect of shadow is not very predictable. For the given conditions, the impact of occultation on an Earth-Moon transfer scenario is summarized in Table 1. In contrast to the observations in the Lyapunov orbit transfer example, the LOSL lunar escape suffers the greatest setback in TOF due to shadow, whereas the VTSL propagation is impacted the least. Here, the TOF increases are more comparable for the VTSL and OFSL enabled Earth escape scenarios. Additionally, between the two sample results, the increase in TOF has varied between 8 and 37 days for the Earth escape phase. So, the change in transfer duration due to occultation events is unpredictable, and is influenced by numerous factors including initial conditions, relative orientation of the sail with respect to the primaries and the Sun line, as well as the steering law. Temperature drops during shadow events could also affect the sail structure and the performance of the on-board instruments.

Impact of Sail Efficiencies

As noted by McInnes,[18] inefficiencies associated with currently available sail materials may be expected on the order of approximately $10 - 15\%$. In this preliminary analysis, the scattering of the incident photons due to surface imperfections is not incorporated. So, although the sail generates a diminished maximum acceleration magnitude due to an efficiency η, implying a value

less than unity in Eqn. (3), the assumption of a perfectly reflecting surface dictates that the sail force acts perpendicular to the sail face. Underperformance of sails is a practical consideration and its impact on the mission outcomes can be explored by re-visiting some of the results generated thus far. During the transfers, the majority of the transfer time involves escaping the gravity well of the Earth. The consequence of introducing sail inefficiencies to this transfer phase is estimated by interpolating and extracting the relevant TOF values associated with the diminished a_c value from the surface plots generated in Fig. 6. For example, Earth escape to a 12-day Lyapunov orbit, using an $a_c = 0.5\ mm/s^2$, and a sail with 85% efficiency, is prolonged by $\approx 0.45\%$ when employing the OFSL, by $\approx 3\%$ when using the LOSL, and the VTSL yields a sacrifice of $\approx 15\%$. These numbers may vary based on the gradient of the TOF surfaces, which are influenced by factors including the initial conditions prior to initiating the spiral and the Sun line position during the escape. However, the TOF surfaces also aid in deducing the order-of-magnitude increases in transfer durations that are attributable to realistic sail inefficiency considerations. These ballpark estimates may be useful when conducting preliminary trades and assessing feasibility. In addition to TOF increases, notice that a reduced sail acceleration magnitude can correspond to a modified baseline geometry.

Sail Turn Rates

In addition to occultation and sail inefficiencies, the turn rate demands placed on a sail also dictate the feasibility of the baseline solutions. Infeasible turn rates can be induced as a result of the inherent logic associated with the specific steering law, as well as the design and implementation choices adopted to generate the baseline solutions. To assess the turn rate limitations, the sail angles acquired from the one-sided sail propagations are converted from the Sun-frame to the Earth-centered inertial frame. Excessive turn rates due to implementation choices are always encountered near the apogee of the spiral trajectories. At these locations, the sail is forcefully feathered, ($n_x = 0$) to reduce the perigee lowering rate and, thereby, prevent an undesirable crash into the primary's surface. As an example, Fig. 10(a) reflects the instantaneous change in direction that may be required to feather the sail under these conditions when employing the VTSL. Similar effects are also observed for the OFSL and the LOSL. When the sail is feathered, the VTSL and LOSL direct the sail normal to trace the velocity components on the $\hat{y} - \hat{z}$ plane. This implementation effort aims to lower the turn rate required to resume acceleration when the sail-active conditions are again satisfied; e.g., when the sail is well past apogee. However, this effort does not eliminate the high turn rates. It is also possible to induce very rapid turns for small variations of the velocity vector across the Sun line. This idea is illustrated in Fig. 10(b). Such an implementation is not even considered with the OFSL because the sail normal must undergo a 90° turn to re-align with the Sun line, regardless of its previous orientation on the $\hat{y} - \hat{z}$ plane.

The steering laws, due to their inherent nature, may not, in fact, be able to satisfy the implementation requirements. The VTSL and OFSL demand that the sail be feathered when moving towards the Sun during an acceleration phase. The transition between the active and feathered states is smooth for the VTSL as the velocity vector itself transitions through the $\hat{y} - \hat{z}$ plane, where $n_x = 0$. In contrast, the OFSL induces high turn rates while feathering/un-feathering the sail because the sail normal is forced to undergo a 90° turn to/from its orientation along the Sun line; Fig. 10(c) demonstrates this scenario. The design of the LOSL allows the sail to remain active to accelerate even when traveling Sunward. However, the sail does come close to being feathered under certain conditions, where the *x*-component of the sail normal, n_x assumes values close to 'zero'. During these instances, the sign on n_y depends on the direction of the deviation of the velocity vector from the negative $\hat{x}$ direction when traveling towards the Sun. This steering law, therefore, induces high-rate

turns that are close to an instantaneous 180° change for very small deviations of the velocity vector across the negative $\hat{x}$ line. This undesired situation, which is intrinsic to the nature of the LOSL, is illustrated in Fig. 10(d). In accordance with Wie et. al,[19] a turn value of 0.02 *deg/s* is identified as a

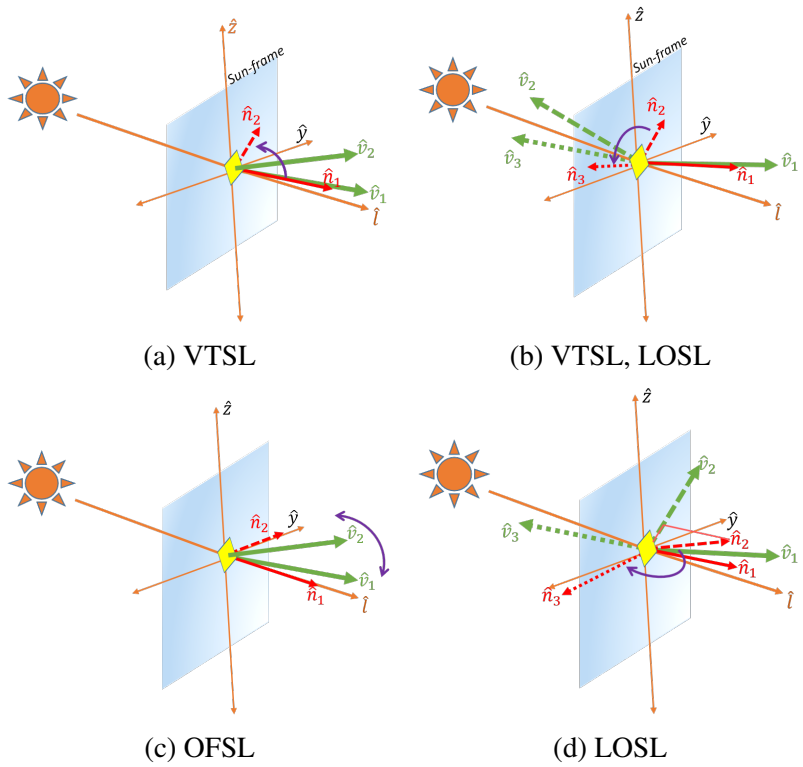

(a) VTSL (b) VTSL, LOSL

(c) OFSL (d) LOSL

Figure 10. Conceptual illustration of high turn rate scenarios: (a) instantaneous feathering near apoapsis affecting all three steering laws (b) tracking velocity components on the $\hat{y} - \hat{z}$ plane when sail is feathered for the VTSL and LOSL (c) high 90° turns inherent to the OFSL logic (d) high turn rate inherent to LOSL logic.

realistic upper bound on acceptable sail turn rates. The demands imposed on the baselines generated thus far are computed by querying the rate of sail orientations every 0.01 *days* (≈ 14.40 *minutes*), or between each integration time-step (whichever is greater). As an example, the high turn rates associated with the spirals generated using all three steering laws from a southern halo manifold at $JC = 3.163$ are illustrated in Figs. 11 and 12. Since the orbital period of the smaller spiral orbits involved is on the order of approximately 10 hours, the query interval of 0.01 days offers sufficient resolution on the turn rate demands. The integration is not conducted at equal time-steps in an attempt to balance accuracy (integration tolerance of $1 \times 10^{-11} ND \approx 0.0038 km$ or $\approx 1.02 \times 10^{-8} m/s$) and computational effort.

The magnitudes of the infeasible turn rates associated with each steering law are represented in Figures 11. The high turn rates might emerge as a result of the design choices, such as the apoapsis cut-off, or result from the normal operation of the steering law for the LOSL and OFSL solutions. Recall that the high turn rates appearing in the VTSL solutions are observed to be solely a result of the implementation choices. In the figure, the dark blue signifies feasible turn rate magnitudes, the red line highlights the upper bound on acceptable turn rates (0.02 *deg/s*), and the other colors represent the high turn rates from propagating the transfer using the increased levels of a_c values

ranging from $0.1 - 0.5\ mm/s^2$. The VTSL and LOSL elicit maximum turns of 0.2 *deg/s*, which correspond to $\approx 173^\circ$ in 14.40 *minutes*. This turn rate is 10 times greater than the feasible 0.02*deg/s*, which is achieved by executing the almost 180° turn in ≈ 2.5 *hours*. The turn rates deemed as infeasible but corresponding to values less than $0.2\ deg/s$, are associated with those computed for time-steps that are greater than 14.40 *minutes* apart, or in which the required turn is $\approx 180^\circ$. The maximum turn rate of 0.1 *deg/s* for the OFSL corresponds to a 90° turn in 14.40 *minutes*, which is also defined as infeasible. However, a turn duration of 1.25 *hours* could reduce the turn rate to 0.02 *deg/s*. The infeasible turn rates with values less than $0.1\ deg/s$ are associated with time-steps that are greater than 14.40 *minutes* apart. Figures 12 displays the locations along the spiral propagations

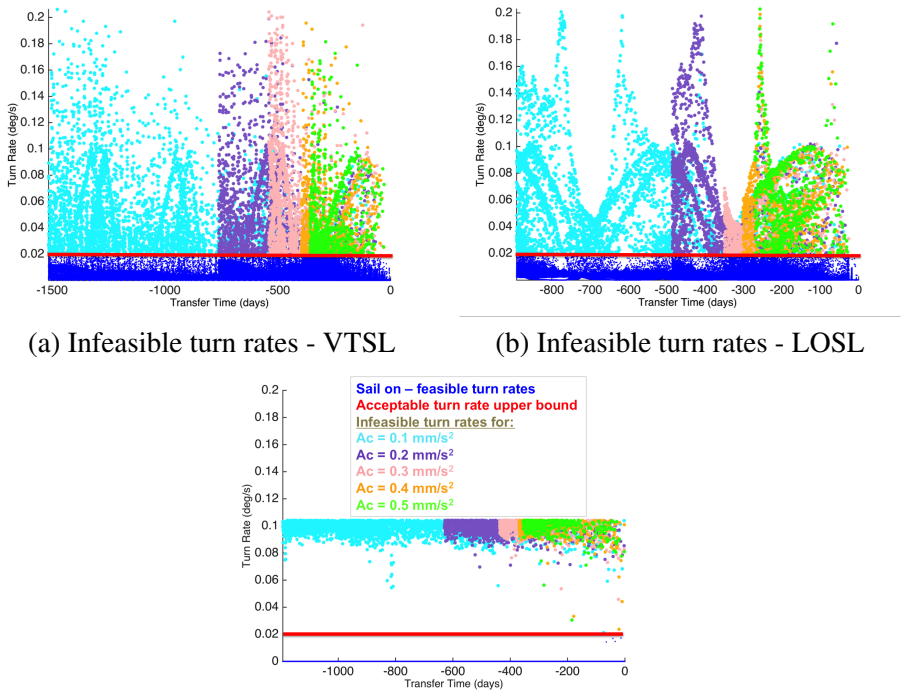

(a) Infeasible turn rates - VTSL

(b) Infeasible turn rates - LOSL

(c) Infeasible turn rates - OFSL

Figure 11. Infeasible turn rate magnitudes associated with all three steering law spiral propagations from a southern halo manifold.

where undesirable turn rates are invoked. When the sail is feathered (off), the displayed path is black, whereas, the active sail trajectory with feasible turn rates, is plotted in blue. Note that sections with feasible turn rates (in blue) are only displayed for the trajectories generated using the lowest a_c value ($0.1\ mm/s^2$), to present a clearer visual. The colored curves highlight where excessive turn rates exist along the propagated path. Two specific patterns are observed - the trajectories possess infeasible turn rates near apogee, and they also possess a sinusoidal pattern of infeasible turn rates all through the spiral phase. The former pattern is identified with the condition where the sail is feathered rapidly when the sail approaches the vicinity of the apogee. The second pattern, however, demonstrates an ≈ 365 day cyclic behavior associated with the infeasible turn rate pattern, which is characteristic to each steering law. During the sidereal period, the continually changing Sun-Earth alignment gradually shifts the location of the infeasible turn rates on each successive orbit. It is interesting to note that only the cyclic trend for the LOSL is comprised of smaller ripples, which have a period close to that of the Sun-Earth-Moon synodic period of approximately

29 days. In this instance, the interplay of the sail acceleration and gravitational influences of the two primaries influence the observed pattern. For the VTSL, the ripples are absent because the high turn rates occur during the sail off stages near apogee, and when moving Sunward. For the OFSL, they occur during transitions, that is, when the sail switches between active/non-active (off) near apogee and when a move Sunward/anti-Sunward is initiated. Translating these baselines to actual

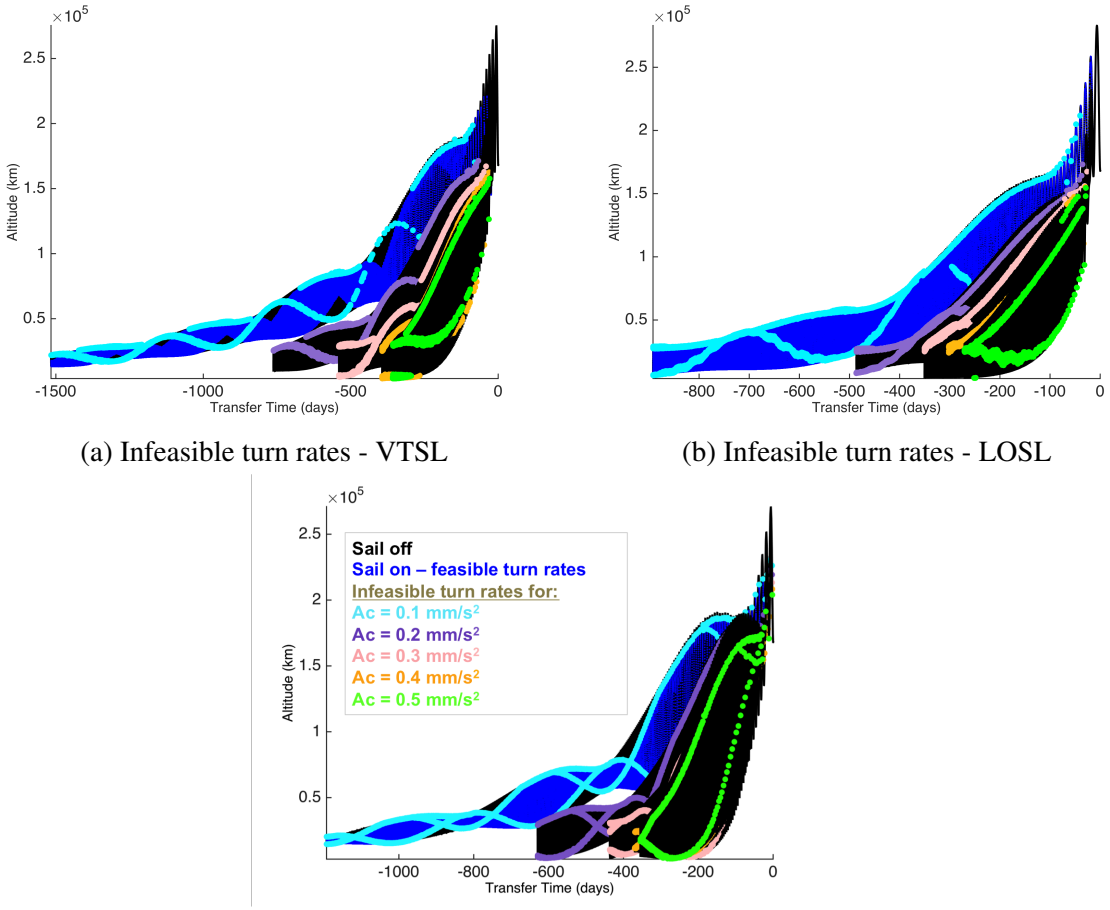

(a) Infeasible turn rates - VTSL

(b) Infeasible turn rates - LOSL

(c) Infeasible turn rates - OFSL

Figure 12. Infeasible turn rate locations associated with all three steering laws; escape spirals from a southern halo manifold in reverse time.

mission scenarios will require addressing the high turn rates issue. The instantaneous high turn rates near apogee must be transitioned to more gradual reorientations and, with active control, to produce a feasible solution.The high turn rates when the sail is feathered on the $\hat{y} - \hat{z}$ plane can be addressed by introducing a control law that maintains a feasible solution without violating the turn rate requirements. Both these issues are concerns introduced by the implementation requirements to generate an acceptable baseline. The turn rates close to 180° for the LOSL to continue accelerating when moving Sunward, and the 90° turns required to transition between the on/off status for the OFSL are concerns inherent to the steering laws, and are more challenging to address. Some high turn rates are also observed at lower perigee altitudes (e.g., for $a_c = 0.5\ mm/s^2$ in Fig. 12(a)), where the sail maneuvers through higher orbital speeds. This physical impingement on the sail turn rate could be addressed by deploying the sail at higher altitudes.

CONCLUDING REMARKS

A renewed interest in returning to the Moon has restored efforts to deliver efficient Earth-Moon transfer mechanisms. Solar sails are an attractive option given their propellant-free transport capability while offering sustained levels of acceleration and the means to support extended mission durations. This preliminary investigation builds on prior work related to low thrust and low energy trajectory concepts to develop a general framework that enables successful solar sail baseline transfers between the Earth and the Lunar region. Multi-body dynamics incorporating the gravitational forces of the Earth and the Moon are exploited to leverage free connecting arcs, such as manifolds, to smoothly insert into a destination orbit. The flexibility of the framework supports sail controlled end-to-end transfers particularly in the absence of natural free connections as well.

Transfer characteristics under different steering strategies are also a consideration. An advantage of the On/Off Steering Law (OFSL) is that it allows the sail to generate the maximum magnitude of acceleration whenever it is active. Accelerating along the direction of motion, however, requires the implementation of the Velocity Tangent Steering Law (VTSL), but at the cost of diminished acceleration magnitudes. Accordingly, the VTSL typically engenders the longest transfer durations. Intrinsic to the construction of the OFSL and VTSL, the inability of the sail to be active to accelerate during Sunward motion also compromises their transfer durations. In contrast, the Locally Optimal Steering Law (LOSL) permits the sail to be active during Sunward motion and executes a less dramatic deviation of the sail normal from the Sun line. So, a typical 4-5 year journey established using a VTSL propagation and current sail acceleration levels ($\approx 0.1\ mm/s^2$), is capable of being shortened by close to half the duration by considering the use of the LOSL. Accomplishing the baseline transfers in the time frame of a year requires more optimistic sail acceleration magnitudes in the range of 0.4-0.5 mm/s^2.

Given any steering law, sail response to realistic mission constraints, such as sail inefficiencies and occultation events, is also assessed. The sail inefficiencies are modeled as a reduction in the maximum acceleration magnitude associated with the sail. So, the resulting geometry of the transfer has the potential to be different from its perfectly efficient counterpart. For some of the cases tested, the inefficiencies have been observed to lengthen the transfer durations by $\approx 15\%$. As the appearances of occultation events are scarce during a given orbit, the geometry of the spirals incorporating them is not usually morphed significantly from their non-shadow counterparts. However, occultations have the potential to lengthen the transfer durations by at least $10-15\%$. Such approximations aid in a more informed time budgeting process during mission design.

The generation of the baseline solutions proves challenging due to the tendency of the perigee to lower rapidly and potentially fall below the planetary radius. An effect well known within the solar sailing community, this issue is addressed by prohibiting the sail from being active within certain specified bounds surrounding the spiral apogees. However, forcing the sail to feather instantaneously from its active pointing direction induces high turn rates. All three steering laws are impacted by this implementation decision. When the sail is feathered, the requirement for the VTSL and LOSL to track the non-Sunward velocity components induces high turn rates. But, this logic is implemented to minimize the sail orientation change required to resume sail acceleration from a feathered state. Such implementation-related infeasible turn rates require further development particularly for higher fidelity solutions. In addition to these implementation-related violations, inherent to the underlying logic, the LOSL inflicts turns close to an instantaneous 180° whilst moving Sunward, and the OFSL inflicts instantaneous 90° turns between its on/off states. So, future work urges the development of control strategies to alleviate the high turn rate requirements whilst still

meeting mission objectives. This current investigation would also benefit from exploring a higher fidelity analysis by incorporating the Sun's gravity, J_2 perturbations and partially lit shadow regions such as the penumbra and antumbra. Additionally, combining the sails with conventional low-thrust engines could shorten the transfer durations and possibly enhance the overall mission.

ACKNOWLEDGEMENTS

The authors wish to acknowledge the support from the School of Aeronautics and Astronautics, and the School of Engineering Education at Purdue.

REFERENCES

[1] N. Sands, "Escape from Planetary Gravitational Fields by Use of Solar Sails," *American Rocket Society Journal*, Vol. 31, 1961, pp. 527–531.

[2] W. R. Fimple, "Generalized Three-Dimensional Trajectory Analysis of Planetary Escape by Solar Sail," *American Rocket Society Journal*, Vol. 32, 1962, pp. 883–887.

[3] L. L. Sackett and T. N. Edelbaum, "Optimal Solar Sail Spiral to Escape," *AIAA/AAS Astrodynamics Specialist Conference and Exhibit*, Jackson Hole, Wyoming, 1977.

[4] A. J. Green, "Optimal Escape Trajectory from a High Earth Orbit by Use of Solar Radiation Pressure," M.S. Thesis, Massachusetts Institute of Technology, 1977.

[5] T. A. Fekete, "Trajectory Design for Solar Sailing from Low-Earth Orbit to the Moon," M.S. Thesis, Massachusetts Institute of Technology, 1991.

[6] V. L. Coverstone and J. E. Prussing, "Technique for Escape from Geosynchronous Transfer Orbit Using a Solar Sail," *Journal of Guidance, Control, and Dynamics*, Vol. 26, July-August 2003, pp. 628–634.

[7] M. Macdonald and C. R. McInnes, "Realistic Earth Escape Strategies for Solar Sailing," *Journal of Guidance, Control, and Dynamics*, Vol. 28, March-April 2005, pp. 315–323.

[8] V. Coverstone-Carroll and J. E. Prussing, "A Technique for Earth Escape Using a Solar Sail," *AIAA/AAS Astrodynamics Specialist Conference and Exhibit*, Girdwood, Alaska, 1999.

[9] J. W. Hartmann, "Escape from Earth using a Solar Sail," Final Report for AAE493 Independent Study, Univ. Of Illinois, Urbana-Champaign, 2003.

[10] M. T. Ozimek, "Low-Thrust Trajectory Design and Optimization of Lunar South Pole Coverage Missions," M.S. Thesis, School of Aeronautics and Astronautics, Purdue University, 2010.

[11] D. J. Grebow, "Trajectory Design in the Earth-Moon system and Lunar South Pole Coverage," M.S. Thesis, School of Aeronautics and Astronautics, Purdue University, 2010.

[12] D. J. Grebow, M. T. Ozimek and K. C. Howell, "Design of Optimal Low-Thrust Lunar Pole-Sitter Missions," *Advances in the Astronomical Sciences*, Vol. 134, February 2009, pp. 741–760.

[13] G. Mingotti and F. Topputo, "Ways to the Moon: A Survey," *Spaceflight Mechanics: Proceedings of the AAS/AIAA Spaceflight Mechanics Meeting*, Vol. 140, No. 3, 2011, pp. 2531–2547.

[14] E. A. Belbruno, "Lunar Capture Orbits, a Method of Constructing Earth Moon Trajectories and the Lunar Gas Mission," *AIAA/DGLR/JSASS International Electric Propulsion Conference*, Colorado Springs, Colorado, 1987.

[15] J. Schoenmaekers, "Post -Launch Optimisation of the SMART-1 Low-Thrust Trajectory to the Moon," *18th International Symposium on Space Flight Dynamics*, Munich, Germany, 2004.

[16] Japan Aerospace Exploration Agency (JAXA), "Small Solar Power Sail Demonstrator, 'IKAROS' - Confirmation of Photon Acceleration," July 2010. `http://global.jaxa.jp/press/2010/07/20100709_ikaros_e.html`; Last Accessed Date: [02 June 2014].

[17] G. G. Wawrzyniak, "The Dynamics and Control of Solar-Sail Spacecraft in Displaced Lunar Orbits," Ph.D. Dissertation, School of Aeronautics and Astronautics, Purdue University, 2011.

[18] C. R. McInnes, *Solar Sailing: Technology, Dynamics and Mission Applications*. Chichester, UK: Praxis, 1999.

[19] B. Wie, "Solar Sail Attitude Control and Dynamics, Part 2," *Journal of Guidance, Control and Dynamics*, Vol. 27, July-August 2004, pp. 536–544.